Analysis of the Dynamic Behavior of Supercritical CO2 Pipeline Based on the Nonisothermal Transient Flow Model

Jia, Qiyun; Li, Yuxing; Hu, Qihui; Zhao, Xuefeng; Yin, Buze; Meng, Lan; Zhu, Jianlu; Lu, Jianxin

DOI
10.1021/acs.energyfuels.4c06010

Publication date
2025

Document Version
Final published version

Published in
Energy and Fuels

energy&fuels

pubs.acs.org/EF

Article

Analysis of the Dynamic Behavior of Supercritical CO_2 Pipeline Based on the Nonisothermal Transient Flow Model

Qiyun Jia, Yuxing Li,* Qihui Hu,* Xuefeng Zhao, Buze Yin, Lan Meng, Jianlu Zhu, and Jianxin Lu

Cite This: *Energy Fuels* 2025, 39, 5463−5478

Read Online

ACCESS | Metrics & More | Article Recommendations

ABSTRACT: In supercritical CO_2 pipeline transport, the operation of pumps and valves often causes the pipeline to enter a transient state. Accurately describing the dynamic response in this state is crucial for making safety control decisions. This paper proposes a nonisothermal one-dimensional transient flow model for supercritical CO_2 pipelines based on one-dimensional transient flow equations and equipment characteristic equations. By comparison with experimental data, the GERG-2008 equation, known for its high accuracy, is chosen to calculate the physical property parameters of CO_2. By comparing with several sets of literature data, the results show that the errors are all within the acceptable range, which verifies the high accuracy of the model. The study investigates the hydraulic and thermal changes in the pipeline under transient operating conditions, including valve closure, slow startup, and sudden shutdown of the centrifugal pump. The results showed that the water-strike intensity of a supercritical CO_2 pipeline is one-third that of a water pipeline but 12 times that of a methane pipeline, which requires sufficient attention. The effect of impurity composition on water strike is significant, particularly when the N_2 content reaches 5%, at which point the maximum pressure decreases by 15.1%. In addition, the timing and method of valve shutoff significantly impact water strikes. It is recommended to prioritize the calculation of piping cycles, determine the maximum valve closing time in conjunction with industry standards, and use a linear valve closing method to reduce the water strike pressure. Studies have shown that the startup or sudden shutdown of centrifugal pumps at the inlet can cause sharp fluctuations in the pressure and flow rate, but the new equilibrium state will be established quickly. In addition, doping reduces the magnitude and rate of pressure changes in the pipeline. This study provides an essential foundation for the safe and stable operation of supercritical CO_2 pipelines.

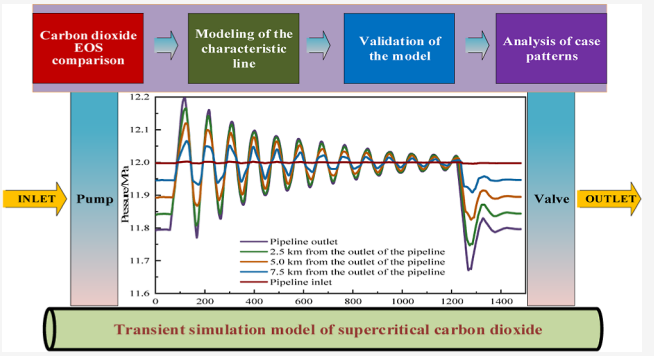

1. INTRODUCTION

Currently, global economic and social development is heavily reliant on fossil energy sources such as coal, crude oil, and natural gas, with the associated energy infrastructure continuing to emit large quantities of greenhouse gases, primarily CO_2, which have severe implications for the climate, environment, and human health.[1] To address global climate change, reduce CO_2 emissions, ensure energy security, and achieve sustainable industrial development, the vigorous promotion of carbon capture, utilization, and storage (CCUS) technology has become essential.[2] CCUS effectively reduces CO_2 emissions to achieve carbon neutrality while supporting high-quality economic and social development.[3] Due to the spatial distribution of CO_2 sources and sinks, pipeline transport will become a critical link connecting the upstream and downstream segments of the CCUS industry chain.[4,5] Pipeline transport of CO_2 differs significantly from natural gas transport as CO_2 is typically in a supercritical or dense phase state.[6] Supercritical CO_2 combines the low viscosity and high fluidity of a gas with the high density of a liquid.[7] This characteristic makes supercritical CO_2 economical for pipeline transport; however, the safety hazards associated with high pressure and high temperature require special attention.[8] Numerical simulation is a cost-effective tool for assessing pipeline operations, particularly useful for countries with limited CO_2 pipeline infrastructure.[9] Developing numerical simulation models for CO_2 pipeline transport is essential for designing and operating CO_2 pipelines safely and economically.

The field of steady-state flow simulation in CO_2 pipelines is now well established. Notable studies in this field include Zhan (2006),[6] McCoy and Rubin (2008),[10] Nimtz (2010),[11] Liu (2013),[12] Liu (2016),[13] and most recently Lu (2021).[14]

Received: December 8, 2024
Revised: February 25, 2025
Accepted: February 28, 2025
Published: March 8, 2025

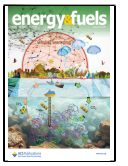

https://doi.org/10.1021/acs.energyfuels.4c06010
Energy Fuels 2025, 39, 5463−5478

Table 1. Density Experiment Data Sources

year	Mixture	temperature/K	pressure/MPa	source
1971	CO_2−N_2, CO_2−CH_4	253−288	2−15	Arai[24]
1988	CO_2, CO_2−CH_4	225−400	2−35	Magee[25]
1997	CO_2−N_2	225−450	1−70	Brugge[26]
2001	CO_2	240−470	0.5−30	Klimeck[27]
2005	CO_2	233−293	0.1−5.7	Saleh[28]
2012	CO_2−O_2	273−293	1−20	Mazzoccoli[29]
2012	CO_2−N_2	250−400	2−20	Mondéjar[30]

Relatively few studies have been conducted on transient flow simulation in CO_2 pipelines. Mahgerefteh et al.[15] developed a one-dimensional computational model for CO_2 pipeline rupture and leakage using the eigenline method. The model accounts for friction between the pipe wall and fluid, heat transfer in the flow, and the effect of pipe diameter on the propagation velocity of the decompression wave after rupture. Munkejord et al.[16] investigated the transport and buckling parameters of a two-phase CO_2−CH_4 mixture and numerically solved the drift flux model using the multistage center (MUSTA) format. The results indicate that the composition of the mix affects its sound velocity and buckling cooling rate. Brown et al.[17] modeled a two-fluid transient flow to simulate the outflow from a high-pressure CO_2 pipeline after failure, where thermal and mechanical nonequilibrium effects during depressurization are explained by a simple ontological relationship describing the transfer of mass, heat, and momentum between phases, i.e., relaxation to equilibrium. Quinn et al.[18] provide an in-depth study of the rapid depressurization behavior of CO_2 using diffuse spot imaging and high-speed photography. Experiments were conducted in specially designed expansion tubes covering a wide range of initial pressure and temperature conditions.

Visualization and velocity analysis of decompression and evaporation waves revealed fluctuation characteristics under varying initial conditions. Clausen et al.[19] used OLGA software to simulate the results of a real 50 km, 24-in.-diameter buried CO_2 pipeline venting under initial supercritical conditions. They found that the impurity content significantly impacts venting behavior, even below 1%. Shang[20] systematically analyzed the hazards of CO_2 leakage and the physical processes involved, including pipeline depressurization, near-field injection, and far-field diffusion. It was concluded that the homogeneous relaxation model and delay homogeneous equilibrium model have significant advantages in terms of prediction accuracy compared to the conventional homogeneous equilibrium model. Chen et al.[21] conducted rupture experiments on an API X52 full-size CO_2 pipeline, tracing in detail the pressure evolution, temperature changes in axial and vertical directions, the micromorphology of the cracks, and the entire process from gas leakage to rupture. The experimental pipeline, designed based on the improved Battelle hyperbolic method (BTCM), validated the developed pressure relief wave prediction model, showing high agreement with experimental data.

Most of the studies mentioned above focus on abnormal operating conditions, such as leakage, depressurization, and blockage, in the CO_2 transport process. However, little research on the CO_2 pipeline transmission under regular operating conditions involves everyday transient events, such as pump station startups and shutdowns, sudden valve closures, and other behaviors resulting from dynamic responses. Chaczykowski and Osiadacz[22] investigated the effects of impurities on pipeline hydraulics during the operation of a supercritical CO_2 pipeline under valve closure and flow rate changes. This study was based on one-dimensional Euler equations, the REFPROP 8.0 database to calculate CO_2 physical properties and relevant derivatives of CO_2, and the linear lines (MOL) method to solve the system of conservation equations. However, the specific effects induced by valve closure and flow rate changes remain understudied, with most research focusing on the impact of impurities. Lu et al.[9] modeled the transient flow of an impurity-containing CO_2 pipeline based on the three significant conservation equations, using the implicit central difference method and the Peng−Robinson equation to describe CO_2's physical properties. The study investigated the effects of outlet flow fluctuations, gas distribution, convergence points, and impurity content on the operation of the CO_2 pipelines under slow transient conditions. However, the developed transient model failed to couple with the pipeline equipment model, limiting its applicability to a single pipeline and restricting the study to simple flow fluctuation conditions. Additionally, the adopted Peng−Robinson equation of state has low accuracy in calculating physical properties. Li et al.[23] developed a transient flow model for a one-dimensional CO_2 pipeline based on the conservation equations for mass, momentum, and energy. They solved the model using the eigenline method to investigate hydraulic and thermal changes along the pipeline under transient conditions, such as fluctuations in the gas source's flow rate and valve openings and closures. However, the study used a simplified set of conservation equations and analyzed the model for only one set of operating conditions, limiting the general applicability of the findings.

This revision enhances readability, clarity, and formal academic tone while maintaining technical precision. In this paper, a one-dimensional nonisothermal transient simulation model of a supercritical/dense-phase CO_2 pipeline is developed by coupling the pipeline transient flow equations, which contain the equations for the conservation of mass, momentum, and energy, with the characteristic equations of the leading pipeline equipment (pumps and valves). The high-precision GERG-2008 natural gas equation of state is used to calculate the physical properties of CO_2, and the equation is discretely solved using the method of characteristics (MOC), which describes the transient behavior of the pipeline with high accuracy. The study focuses on the transient changes of hydraulic and thermal forces along the pipeline under dynamic conditions such as valve closure, slow startup, and sudden shutdown of the pumping station, and based on this, corresponding engineering optimization recommendations are made to improve the safety and operational efficiency of the pipeline system.

2. MODEL

2.1. Transient Flow Modeling of Pipelines. The equations for conservation of mass, momentum, and energy form a set of equations for the control of one-dimensional

https://doi.org/10.1021/acs.energyfuels.4c06010
Energy Fuels 2025, 39, 5463−5478

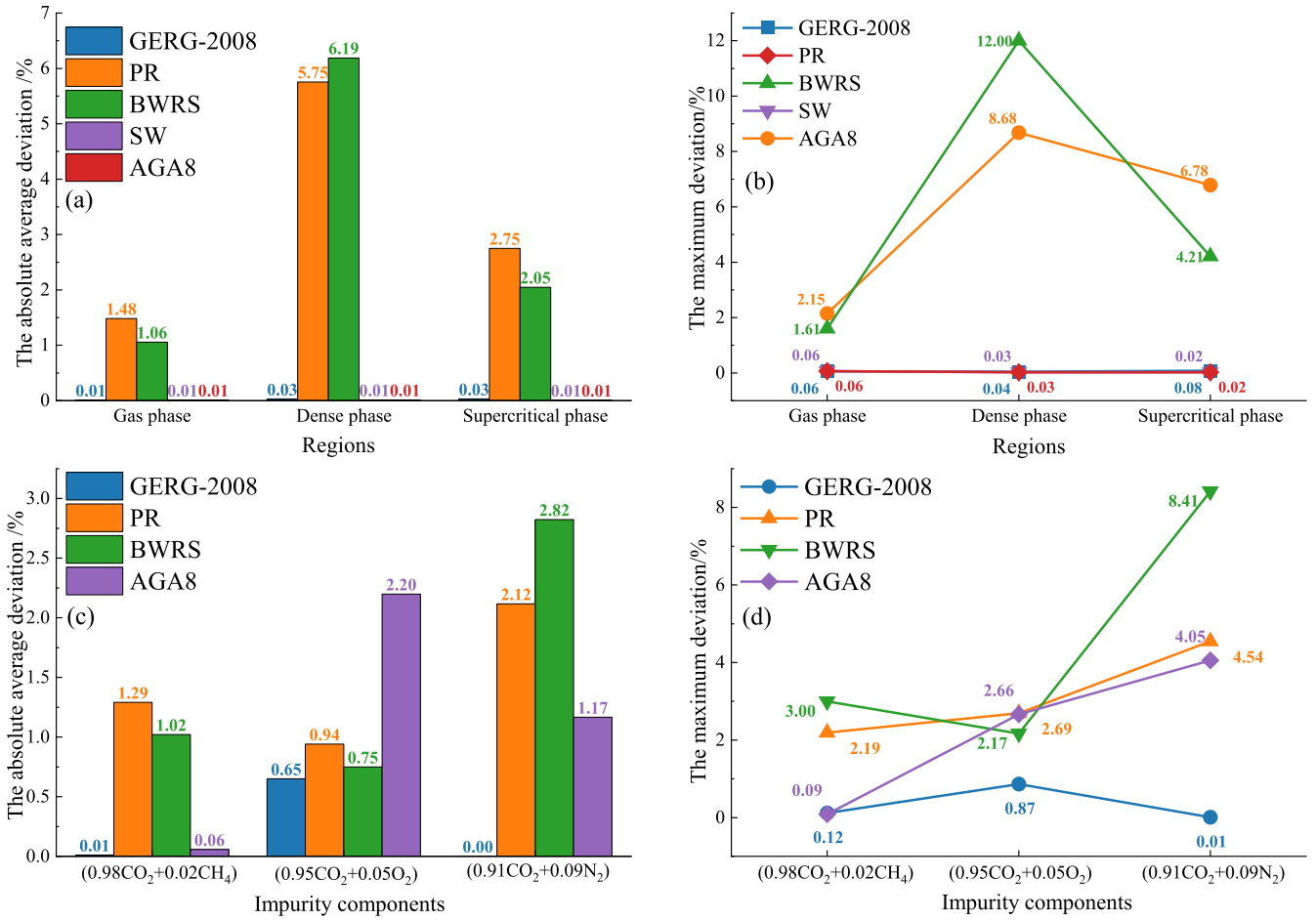

Figure 1. Comparison of calculation results of different equations of state with experimental density data.

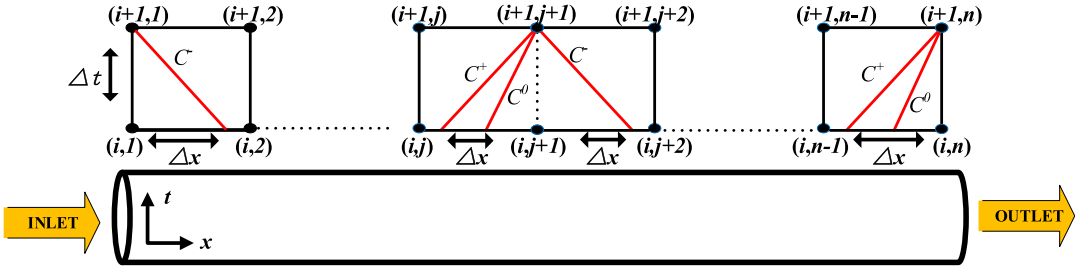

Figure 2. Schematic diagram of feature line meshing.

compressible flow under nonisothermal conditions in a carbon dioxide pipe with the following expressions

$$\frac{\partial \rho}{\partial \tau} + \frac{\partial(\rho v)}{\partial x} = 0 \tag{1}$$

$$\frac{\partial(\rho v)}{\partial \tau} + \frac{\partial(\rho v^2)}{\partial x} + \rho g \frac{\mathrm{d}s}{\mathrm{d}x} + \frac{\partial p}{\partial x} + \frac{\lambda}{D}\frac{\rho v^2}{2} = 0 \tag{2}$$

$$\frac{\partial}{\partial \tau}[\rho(u + v^2/2 + gs)] + \frac{\partial}{\partial x}[\rho v(h + v^2/2 + gs)] + \rho v \frac{\partial q}{\partial x} = 0 \tag{3}$$

where ρ is the fluid density, kg/m^3; v is the fluid velocity, m/s; x is the axial length of the pipe, m; τ is a time variable, s; s is the pipeline elevation, m; g is the acceleration of gravity, m/s^2; p is the pressure of fluid medium, pa; λ is the friction coefficient, dimensionless; d is the inner diameter of the pipe, m; u is the internal energy of fluid, J/kg; h is the enthalpy of fluid, J/kg; q is the heat transfer, J.

Equation 3 is expressed as the heat transfer variation caused by the heat conduction between the pipeline and the surrounding environment. The calculation expression in the pipeline is as follows

$$\frac{\partial q}{\partial x} = \frac{4K(T - T_{amb})\pi D}{\rho v \pi D^2} = \frac{4K(T - T_{amb})}{\rho v D} \tag{4}$$

where T is the gas temperature, K; T_{amb} is the temperature at the buried depth of the pipeline, and K is the total heat transfer coefficient, W/(m^2·K).

The elevation phase in Formula 3 can be integrated as follows

https://doi.org/10.1021/acs.energyfuels.4c06010
Energy Fuels 2025, 39, 5463−5478

$$\rho\frac{\partial(gs)}{\partial\tau} + \rho v\frac{\partial(gs)}{\partial x} = \frac{mg}{A}\frac{\mathrm{d}s}{\mathrm{d}x} \tag{5}$$

According to the general relationship of thermodynamics, the internal energy is transformed into the relationship among enthalpy, pressure, and density

$$h = u + \frac{P}{\rho} \tag{6}$$

By integrating formula 4, formula 5, and formula 6 into formula 3, we obtained the variation form of the energy conservation equation

$$\frac{\partial}{\partial\tau}\left[\rho\left(h - \frac{P}{\rho} + v^2/2\right)\right] + \frac{\partial}{\partial x}[\rho v(h + v^2/2)] = -\frac{4K(T - T_{amb})}{D} - \frac{mg}{A}\frac{\mathrm{d}s}{\mathrm{d}x} \tag{7}$$

The CO_2 pipeline conveying process uses the mass flow rate to represent delivery capacity, leading to the concept of mass flow rate, such that $m = \rho vA$. Simultaneously, the system of control equations is transformed into a set of equations with temperature T, pressure P, and mass flow rate m as the primary variables according to the mathematical relations.

$$\left(\frac{\partial\rho}{\partial p}\right)_T\frac{\partial P}{\partial\tau} + \left(\frac{\partial\rho}{\partial T}\right)_P\frac{\partial T}{\partial\tau} + \frac{1}{A}\frac{\partial m}{\partial x} = 0 \tag{8}$$

$$\left[1 - \frac{m^2}{A^2\rho^2}\left(\frac{\partial\rho}{\partial P}\right)_T\right]\frac{\partial P}{\partial x} - \frac{m^2}{A^2\rho^2}\left(\frac{\partial\rho}{\partial T}\right)_P + \frac{1}{A}\frac{\partial m}{\partial\tau} + \frac{2m}{\rho A^2}\frac{\partial m}{\partial x} + \frac{\lambda m^2}{2\rho DA^2} + \rho g\frac{\mathrm{d}s}{\mathrm{d}x} = 0 \tag{9}$$

$$\left[\rho\left(\frac{\partial h}{\partial P}\right)_T - 1\right]\frac{\mathrm{d}P}{\mathrm{d}\tau} + \rho\left(\frac{\partial h}{\partial T}\right)_P\frac{\mathrm{d}T}{\mathrm{d}\tau} - \frac{\lambda m^3}{2DA^3\rho^3} + \frac{4K(T - T_{amb})}{D} = 0 \tag{10}$$

2.2. Physical Property Calculation Model. *2.2.1. Selection of Absolute Gas State Equation.* Carbon dioxide has a variety of phases, including gaseous, liquid, solid, supercritical, and dense phases. The physical characteristics of these phases differ significantly, and the physical parameters can change drastically in the critical region. Therefore, selecting high-precision equations of state is essential to accurately describe and predict the behavior of CO_2 under different conditions. A variety of equations of state have been available for calculating the physical properties of CO_2, among which the more commonly used ones include the Peng−Robinson equation, the BWRS equation, the AGA8 equation, the GERG-2008 equation, and the Span-Wagner equation, which is specifically designed for the calculation of the physical properties of pure CO_2. To select the most suitable equation of state for calculating the physical properties of CO_2, the computational accuracy of these five equations will be evaluated in this paper using the density experimental data from references. The specific data sources are listed in Table 1.

Figure 1 illustrates the average and maximum errors for pure CO_2 in different phases and CO_2 systems containing impurities. The AGA8, GERG-2008, and Span−Wagner equations of state demonstrate high accuracy in the density calculations of pure CO_2, with average errors below 0.03% and maximum errors not exceeding 0.08%. In contrast, the PR and BWRS equations of state exhibited higher errors, particularly in the dense phase region, where the maximum error of BWRS could reach up to 12%. The Span−Wagner equation of state is excluded from the comparison for CO_2 mixtures as it only applies to pure CO_2 property calculations. Overall, the PR and BWRS equations of state still exhibit non-negligible errors. Although the AGA8 equation of state demonstrates high accuracy in pure CO_2 density calculations, it also shows some errors. Only the GERG-2008 equation of state consistently maintains high accuracy, with an average error not exceeding 0.65%. This equation can accurately calculate the mobile phases of gas, liquid, supercritical states, and gas−liquid equilibrium, demonstrating excellent accuracy in estimating the physical parameters of pure CO_2 or CO_2 mixtures. Based on the above analysis, this paper selects the GERG-2008 equation for subsequent calculations to ensure high accuracy in the physical property calculations of CO_2.

Although the GERG-2008 equation of state exhibits high accuracy and broad applicability in the natural gas sector, it still has significant limitations. First, the equation is primarily optimized for standard gas components (methane, ethane, nitrogen, and carbon dioxide). However, it lacks sufficient experimental data for atypical impurities (argon, helium, hydrogen sulfide, and heavy hydrocarbons), which may reduce its accuracy in predicting these mixtures. Second, the equation is valid within a temperature range of 90−450 K and a pressure range of 0−35 MPa. Its accuracy may decline when applied beyond these limits.[31] Additionally, although GERG-2008 performs well in gas, liquid, and supercritical phases, its reliance on extrapolated mixing rules for predicting gas−liquid equilibrium states may introduce deviations in density and phase boundary predictions, particularly in near-critical regions. For example, the model inaccurately describes the carbon dioxide mixtures' phase boundaries and water's gas solubility.[32] Therefore, the applicability and limitations of this equation of state should be carefully considered when employing it in calculations in this study.

2.2.2. Viscosity Calculation Method. In pipeline transportation systems, fluid viscosity is the primary factor influencing hydraulic losses along the route. Generally, increased viscosity results in a higher frictional resistance, leading to a more significant pressure drop within the pipeline system. Therefore, in supercritical CO_2 pipeline simulations, accurately calculating fluid viscosity is essential for predicting pressure loss variations along the pipeline.

A literature review indicates the modified formula proposed by Fenghour et al.[33] Fenghour's method, which refines the original viscosity calculation by incorporating the effects of density and temperature on residual viscosity, exhibits high accuracy. This method achieves a maximum relative deviation of no more than 0.5% in the CO_2 viscosity calculations. Consequently, this study adopts Fenghour's method for viscosity calculations of CO_2 fluids using the following equations

$$\eta(\rho, T) = \eta_0(T) + \Delta\eta(\rho, T) + \Delta\eta_c(\rho, T) \tag{11}$$

https://doi.org/10.1021/acs.energyfuels.4c06010
Energy Fuels 2025, 39, 5463−5478

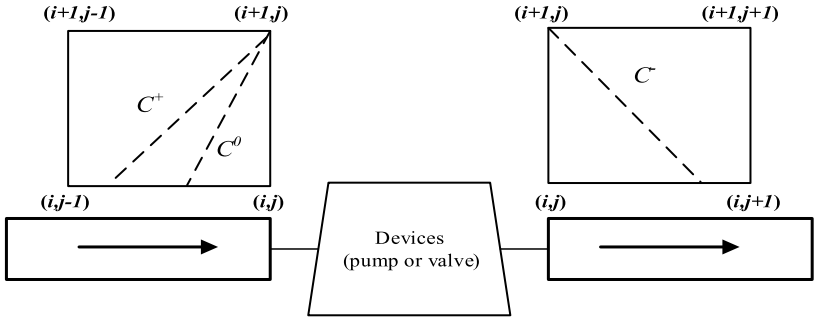

Figure 3. Schematic diagram of device boundary conditions.

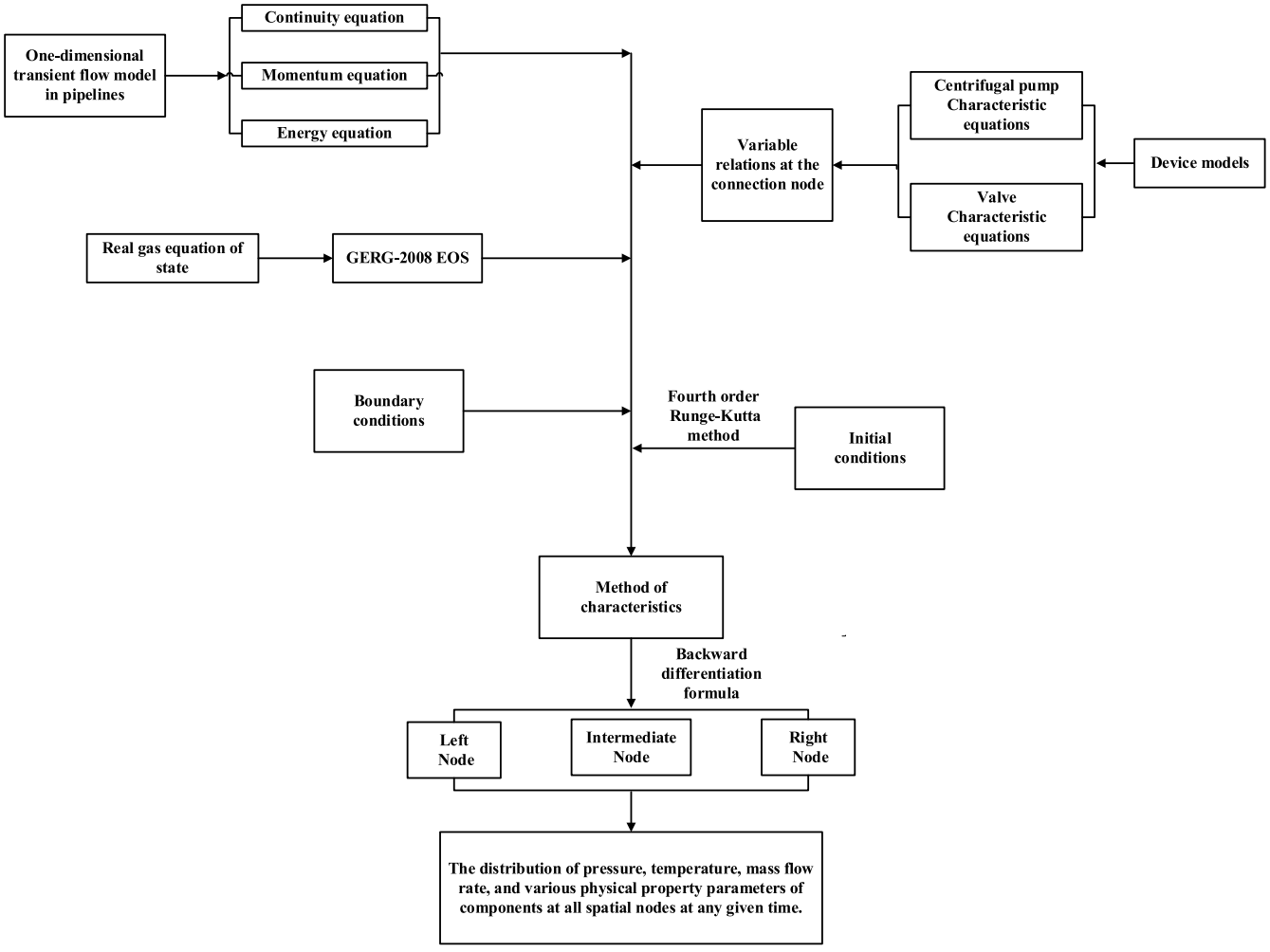

Figure 4. Framework of the CO_2 pipeline transient simulation model.

$$\eta_0(T) = \frac{1.00697T^{0.5}}{\xi_\eta^*(T^*)},\ \ln \xi_\eta^*(T^*) = \sum_{i=0}^{4} a_i(\ln T^*)^i,\ T^* = \frac{kT}{\varepsilon} \tag{12}$$

$$\Delta\eta(\rho, T) = d_{11}\rho + d_{21}\rho^2 + \frac{d_{64}\rho^6}{T^{*3}} + d_{81}\rho^8 + \frac{d_{82}\rho^8}{T^*} \tag{13}$$

where $\eta(\rho,T)$ is the viscosity, μPa·s; $\eta_0(T)$ is the zero-density limiting viscosity, μPa·s; $\Delta\eta(\rho,T)$ is the excess viscosity, μPa·s; $\Delta\eta_c(\rho,T)$ is a critical enhancement effect, which, according to Vesovic's study, is so weak that it can be ignored in the overall viscosity calculation, and therefore is not considered in this paper;[34] ρ is the density, kg/m^3; T is the temperature, K; ε/k is the energy scale parameter, dimensionless; a_i, d_{11}, d_{21}, d_{64}, d_{81}, and d_{84} are fit coefficients to the experimental data, dimensionless.

2.3. Modeling of Pipeline Equipment. *2.3.1. Pump.* Due to the liquid-like properties of supercritical/dense-phase CO_2, centrifugal pumps are commonly used in engineering applications as pressurization equipment for CO_2 pipelines to overcome along-stream friction and flipping points. The equation for the pressure provided by a centrifugal pump at variable speed is as follows

https://doi.org/10.1021/acs.energyfuels.4c06010
Energy Fuels 2025, 39, 5463−5478

$$P_{out} - P_{in} = \rho g\left[A\left(\frac{N}{N_{rate}}\right)^2 + B\left(\frac{N}{N_{rate}}\right)Q_v + CQ_v^2\right] \quad (14)$$

where P_{out} is the pump outlet pressure, pa; P_{in} is the pump inlet pressure, pa; ρ is the density of the medium, kg/m^3; g is the acceleration of gravity, m/s^2; Q_v is the volume displacement of the pump, m^3/h; A, B, and C according to the pump characteristic curve using the least-squares method of fitting the constant coefficient; N is the actual speed of the pump, rpm; and N_{rate} is the rated speed of the pump, rpm.

CO_2 in the pump through the time is very short, the heat is too late to dissipate, and the pressure rise process can be approximated as reversible adiabatic compression, i.e., isentropic. As a result, the compression temperature increase equation can be established as follows

$$\ln\left(\frac{T_{out}}{T_{in}}\right) = \frac{\beta_p v(P_{out} - P_{in})}{C_p} \quad (15)$$

where T_{out} is the pump outlet temperature, K; T_{in} is the pump inlet temperature, K; β_p is the coefficient of thermal expansion, 1/K; v is the specific volume of CO_2, m^3/kg; and C_p is the specific heat capacity of CO_2, J/(kg·K).

The mass flow rate before and after pump satisfies the following flow balance equation

$$M_{in} = M_{out} \quad (16)$$

2.3.2. Valve. A valve is a crucial device to regulate fluid pressure and flow in a CO_2 pipeline, which controls the liquid state by adjusting the opening. The relationship between mass flow rate, pressure, and temperature at different openings is expressed as follows

$$Q = C_d A_f \sqrt{\frac{2(P_{in} - P_{out})}{\rho}} \quad (17)$$

$$T_{in} - T_{out} = \frac{(D_{in} + D_{out})}{2}(p_{in} - p_{out}) \times 10^{-6} \quad (18)$$

$$M_{in} = M_{out} \quad (19)$$

where Q is the valve volume flow, m^3/h; C_d is the valve flow coefficient, with the change of opening and change; A_f is the valve overflow area, m^2; D_{in}, D_{out} is the valve inlet and outlet Joule-Thomson coefficient, K/MPa; P_{out}, P_{in} are the valve inlet and outlet pressure, pa; T_{in}, T_{out} are valve inlet and outlet temperatures, K; and M_{in}, M_{out} are valve inlet and outlet mass flow rates, respectively, kg/s.

3. SOLUTION METHOD

The set of fundamental pipeline transient equations and the accurate gas equation of state form a closed set of equations describing the unsteady flow in supercritical CO_2 pipelines. Since this system of equations is formally a hyperbolic partial differential equation, it is not easy to solve analytically, so numerical methods are required. Among many numerical methods, MOC is particularly effective because it uses wave propagation characteristics to construct differential equations.[35] Compared with the finite-difference method, MOC has a significant advantage in accuracy and is widely used in transient analysis. In this paper, we will use the characteristic line method to transform the system of partial differential equations into a system of ordinary differential equations along the characteristic line for solving to improve the accuracy and efficiency of the calculation.

3.1. Characteristic Difference Equations. A series of variations (eqs 8−10) are used to obtain the system of ordinary differential equations using the eigenline method, and the system of ordinary differential equations is numerically discretized using the explicit difference format. The pipeline segment discretization and the eigenline network division are shown schematically in Figure 2. Subject to the Courant−Friedrich−Levy (CFL)[36] stability criterion, the expression of the characteristic difference equation is as follows

$$AA_1P_4 - BB_1T_4 + CC_1m_4 = DD_1\Delta\tau + AA_1P_1 - BB_1T_1 + CC_1m_1 \quad (20)$$

$$EE_2P_4 + BB_2T_4 - CC_2m_4 = FF_2\Delta\tau + EE_2P_2 + BB_2T_2 - CC_2m_2 \quad (21)$$

$$GG_3P_4 + HH_3T_4 = KK\Delta\tau + GG_3P_3 + HH_3T_3 \quad (22)$$

Among them

$$AA = \left[1 - \left(\frac{\partial\rho}{\partial P}\right)_T \frac{ma_s}{\rho A}\right] \quad BB = \left(\frac{\partial\rho}{\partial T}\right)_p \frac{ma_s}{\rho A}$$

$$CC = \frac{a_s}{A} \quad EE = \left[1 + \left(\frac{\partial\rho}{\partial P}\right)_T \frac{ma_s}{\rho A}\right]$$

$$DD = \frac{4K(T - T_{amb})a_s^2(\partial\rho/\partial T)_p}{\rho c_p D} - \frac{\lambda m^3 a_s^2(\partial\rho/\partial T)_p}{2DA^3\rho^3 c_p} - \frac{\lambda m^2 a_s}{2DA^2\rho} - \rho g a_s \frac{ds}{dx}$$

$$FF = \frac{4K(T - T_{amh})a_s^2(\partial\rho/\partial T)_p}{\rho c_p D} - \frac{\lambda m^3 a_s^2(\partial\rho/\partial T)_p}{2DA^3\rho^3 c_p} + \frac{\lambda m^2 a_s}{2DA^2\rho} + \rho g a_s \frac{ds}{dx}$$

$$GG = \left[\rho\left(\frac{\partial h}{\partial P}\right)_T - 1\right] \quad HH = \rho\left(\frac{\partial h}{\partial T}\right)_p$$

$$KK = \frac{\lambda m^3}{2DA^3\rho^2} - \frac{4K(T - T_{amb})}{D}$$

3.2. Boundary Conditions. The boundary condition is the key to determining the simulation model's unique solution, which describes the operation state of the boundary nodes in the whole time domain. As shown in Figure 2, only 1 or 2 feature lines intersect the boundary at both ends for the pipeline simulated by the feature line method. Both need to determine flow parameters, such as temperature (T), pressure (P), and mass flow rate (m) at the boundary location by adding boundary conditions. In practical engineering applications, the following everyday situations usually exist (Figure 3):

(1) It is known that the upstream end is the gas source point, then the temperature and pressure at the gas source at the upstream end are known quantities:

$$P = \text{const}, \quad T = \text{const} \quad (23)$$

https://doi.org/10.1021/acs.energyfuels.4c06010
Energy Fuels 2025, 39, 5463−5478

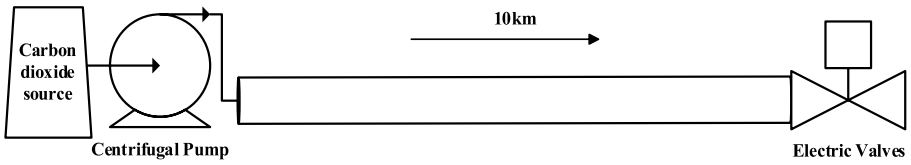

Figure 5. Schematic diagram of the pipeline structure in the case study.

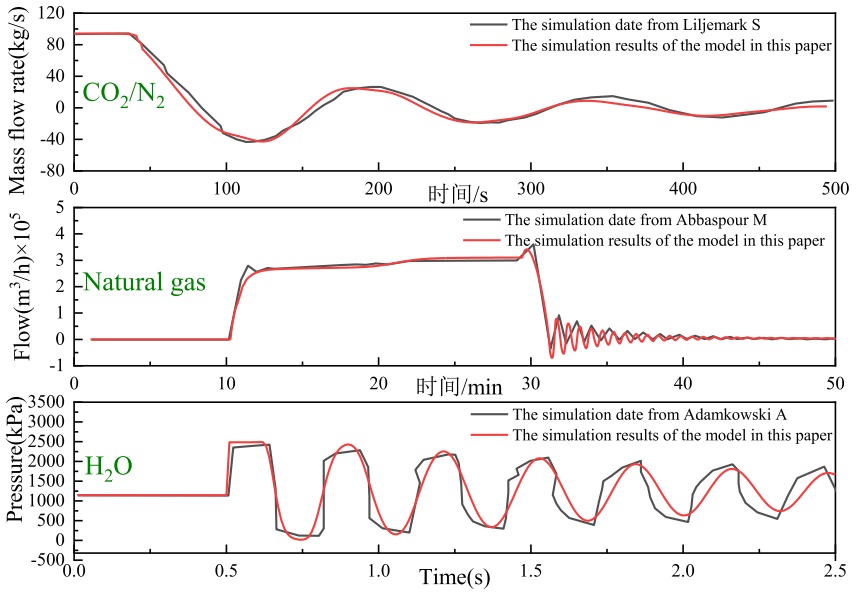

Figure 6. Model comparison validation plot.

(2) If the flow rate downstream of a pipe is a function of time, then the flow rate at each moment downstream is known, and a functional relationship exists:

$$Q = f(\tau) \tag{24}$$

(3) With the existence of pumps, valves, and other equipment in the pipeline, it is necessary to increase the number of calculation nodes, and the inlet and outlet of the equipment are connected to different characteristics of the line; you can select the speed of the pump and the time-varying function of the valve opening as the internal boundary conditions to control the operation of the pumps and valves.

3.3. Initial Conditions. In practical applications of transient simulations in a one-dimensional pipeline, steady-state conditions are typically used as the initial conditions. This paper introduces the fourth-order Runge−Kutta method, which is high in precision, simple to implement, and computationally efficient in solving for steady-state conditions. The expression is as follows

$$y_{k+1} = y_k + \frac{\Delta x_k}{6}[R_1 + 2R_2 + 2R_3 + R_4] \tag{25}$$

where x_k is the computational step; R is the derivative of each unknown of the differential equation concerning x; the subscripts 1, 2, 3, and 4 are the orders of the derivatives appearing in that differential equation. The specific formula is as follows

$$\begin{aligned} R_1 &= f(x_k, y_k) \\ R_2 &= f\left(x_k + \frac{\Delta x_k}{2}, y_k + \frac{\Delta x_k}{2}\cdot R_1\right) \\ R_3 &= f\left(x_k + \frac{\Delta x_k}{2}, y_k + \frac{\Delta x_k}{2}\cdot R_2\right) \\ R_4 &= f(x_k + \Delta x_k, y_k + \Delta x_k \cdot R_3) \end{aligned} \tag{26}$$

3.4. Modeling Framework for the Nonisothermal Transient Flow of CO_2. In this paper, a one-dimensional nonisothermal CO_2 pipeline transient flow simulation model is constructed for simulating the dynamic changes of temperature, pressure, mass flow rate, and medium parameters at each discrete node in the pipeline with time. Figure 4 illustrates the framework of the transient simulation model for the CO_2 pipeline. The model's core is a one-dimensional pipeline characteristic, including continuity, momentum, and energy. Meanwhile, the operating characteristic equations of centrifugal pumps and valves are considered for boosting and regulating devices. At the equipment connection nodes, variable relationship equations were introduced to ensure unity of the whole CO_2 piping system. At each discrete node, the physical parameters of CO_2 were calculated by using the GERG-2008 equation of state. The differential equations for the pipe segments are discretized using the eigenline method and solved using the inverse step method to obtain the distribution of pressure, temperature, mass flow rate, and medium parameters at each discrete moment. The overall numerical model will be implemented in the Visual Studio 2017 environment using the C ++ programming language.

https://doi.org/10.1021/acs.energyfuels.4c06010
Energy Fuels 2025, 39, 5463−5478

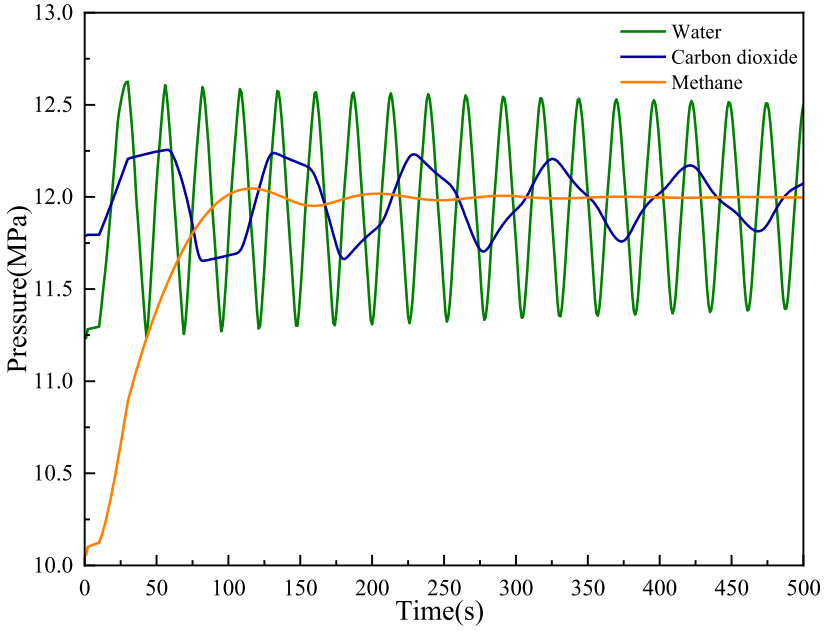

Figure 7. Pressure change curves of different media at the valve after sudden closure of the valve.

4. CASE STUDY

To fit the background of the engineering study, a high-pressure CO_2 transport pipeline in China with a delivery scale of one million tonnes will be used as the basis for setting the case parameters. The structure schematic of the CO_2 pipeline for the case study is shown in Figure 5, which contains a centrifugal pump at the inlet of the pipeline and an electric valve at the outlet of the pipeline. The length of the pipeline is 10 km, regardless of topographic relief, the diameter of the pipe is 324 mm, the wall thickness is 12 mm, the absolute roughness inside the pipe is 5×10^{-5} m, the assumed soil depth is 1.5 m, and the average soil temperature is 293.15 K. The soil thermal conductivity is 1.65 W/(m·K).

4.1. Model Validation. Currently, experimental and field engineering data on transient transportation in supercritical CO_2 pipelines are still scarce, and the research literature on the phenomenon of water strikes in supercritical CO_2 pipelines is limited. In order to verify the accuracy of the established model, three different media, namely, CO_2/N_2 mixture, natural gas, and H_2O, are selected for pipeline transient transport simulation and compared and analyzed with the literature data of Liljemark et al.,[37] Abbaspour and Chapman,[38] and Adamkowski and Lewandowski[39] to assess the validity and accuracy of the model.

Among these studies, Liljemark et al. simulated the change in mass flow rate within a pipeline under supercritical conditions for a CO_2/N_2 fluid mixture containing 98% CO_2 in a 31.2 km long segmented pipeline when the valves were rapidly closed. Using an established nonisothermal model, Abbaspour and Chapman simulated the inlet volume flow rate of a natural gas fluid in a 5 km long pipeline caused by the sudden opening and closing of end valves. Adamkowski and Lewandowski conducted a water hammer experiment in a 98.11 m long experimental pipeline to study pressure fluctuations in the transmission pipeline. A comparison of the model's calculation results with literature data is shown in Figure 6.

It can be observed that when a valve in the pipeline is suddenly closed, it triggers periodic fluctuations in pressure and flow rate, a phenomenon verified under all three simulated conditions. The model's results in this study align closely with the trends observed in the three literature data sets, with the numerical results being broadly consistent. Specifically, compared to Liljemark S's data, the average error in peak flow fluctuation is 11.81%, and the average error in the fluctuation period is 10.53%. Compared to Abbaspour M's data, the average error in peak flow fluctuation is 5.78%, and the average error in the fluctuation period is 6.67%. Compared to Adamkowski A's experimental data, the average error for peak pressure fluctuation is 5.62%, and the average error for the fluctuation period is 3.35%. The model's results are consistent with the literature data, and the error range meets engineering requirements. This indicates that the one-dimensional nonisothermal CO_2 pipeline transient flow simulation model established in this paper has high accuracy and can be applied to calculating transient conditions in CO_2 pipelines.

4.2. Sudden Closure of Valves. This section aims to investigate the hydraulic and thermal changes induced by pipeline valve closing operations, focusing on demonstrating the drastic degree of valve water strike in a supercritical CO_2 pipeline and the influence of relevant factors on the maximum valve water strike pressure in a supercritical CO_2 pipeline, with the study scenario based on the pipeline structure shown in Figure 5. The change of the opening in the valve characteristic eq controls the closing of the valve. The working base conditions of the pipeline inlet temperature of 40 °C, inlet pressure of 12 MPa, and outlet flow rate of 60 kg/s are kept constant.

4.2.1. Pipeline Valves for Different Media Water Impact. To demonstrate the significant effect of the water hammer at the valve of a CO_2 pipeline, we simulated the transient pressure changes of three media—water, carbon dioxide, and methane—during 20 s of valve closure. As shown in Figure 7, when the valve closes, the sudden change in flow rate causes a rapid shift in the fluid's kinetic energy, generating a pressure wave that reflects back and forth, resulting in sharp pressure fluctuations inside the pipe. During propagation, the pressure wave is affected by friction and energy dissipation, gradually weakening before eventually stabilizing. The pressure fluctuations at the valve vary significantly among different media. Under the same operating

https://doi.org/10.1021/acs.energyfuels.4c06010
Energy Fuels 2025, 39, 5463−5478

conditions, the maximum water hammer pressure of supercritical CO_2 is 0.46 MPa, approximately 12 times that of methane and one-third that of the water pipeline. This is because the density and pressure wave velocity of supercritical CO_2 are lower than water's. Although the pressure wave velocity of CO_2 is similar to that of methane, its density is much higher than methane's. Therefore, the same flow rate variation results in the maximum water hammer pressure difference noted above. Regarding the water hammer period, the fluctuation period for supercritical CO_2 and methane is approximately the same, 97 s, significantly slower than that of the water pipeline, which is about three times longer. This is because the pressure wave speeds of supercritical CO_2 and methane are similar, though lower than that of water. In conclusion, the extent of water hammer pressurization in supercritical CO_2 pipelines is lower than that in water pipelines, and the resulting shock frequency is slower. However, it is still more significant than methane pipelines and should not be overlooked.

To analyze the distribution of the water-strike pressure along the CO_2 pipeline, we pooled the pressure data at 0, 2.5, 5, 7.5, and 10 km from the outlet (Figure 8). The pressure fluctuations

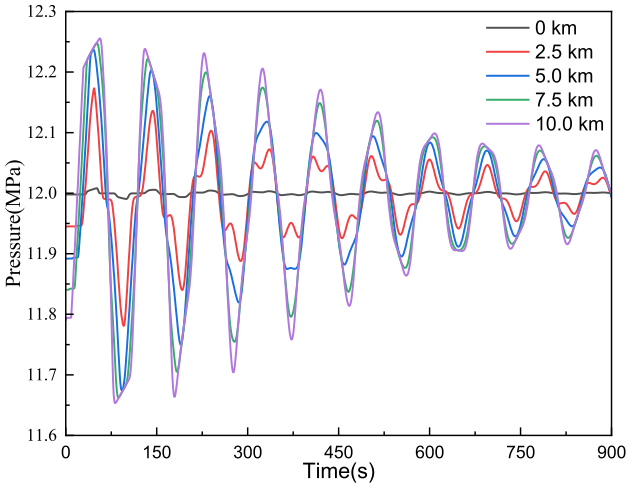

Figure 8. Pressure variation curves at different locations of the pipe.

at different locations of the pipeline show the same fluctuation period and fluctuation amplitude with variability, with the maximum water strike pressure reaching 0.46 MPa at 10 km, decreasing to 0.4 MPa at 7.5 km, 0.34 MPa at 5 km, 0.23 MPa at 2.5 km, and finally 0.01 MPa at 0 km and the outlet. It can be seen that the maximum water strike pressure occurs at the valve; the farther away from the valve, the water strike pressure generated will gradually decrease, so the pipeline inlet pressure is basically in a stable state. After the valve is closed, the fluid near the valve first stops flowing, generating shock and leading to fluid compression, which causes the pressure to rise. Then, subsequent fluids gradually stop flowing, and shocks are applied to the fluid in front of them, further triggering compression and increased pressure. This progressive effect maximizes the water strike pressure at the valve.

4.2.2. Effect of Different Impurities on the Water Strike of Pipeline Valves. In practice, CO_2 pipelines usually do not guarantee the purity of the transported CO_2, and impurities may significantly affect its thermophysical properties and flow characteristics during pipeline transport.[40] To investigate the effect of impurity components on the water strike pressure at the pipeline valves, the three most common impurities (O_2, CH_4, and N_2) were selected. By investigating famous CCS projects such as Dynamis (EU),[41] Porthos (NL),[42] and the technical reports published by NETL (2019)[43] and ISO (2016)[44] on the design parameters of impurities for CO_2 pipeline transportation, it was found that the purity of CO_2 medium has a requirement of no less than 95%, so the maximum doping ratio was set to 5%, and 1%, 3%, and 5% doping contents were set for the study.

Figure 9 illustrates the pressure fluctuations at the valve after the valve is closed for pure CO_2 and for CO_2 mixtures doped with different proportions of O_2, CH_4, and N_2. It can be observed that the addition of these three impurities results in a decrease in the maximum pressure at the valve and an increase in the fluctuation period. Among them, the N_2 impurity has the most significant impact, followed by O_2, with CH_4 having the least effect. This influence intensifies as the impurity content increases. Taking the simulation results for 5% impurity content as an example, under the same working conditions, a 5% N_2 impurity causes a 15.1% decrease in the maximum pressure and a 35.4% increase in the fluctuation period; a 5% O_2 impurity leads to an 11.6% decrease in the maximum pressure and a 29.2% increase in the fluctuation period; a 5% CH_4 impurity results in a 7.5% decrease in the maximum pressure and an 18.8% increase in the fluctuation period. This is because these gaseous impurities, unlike supercritical CO_2, lack near-liquidlike properties, making them more compressible and less dense. Incorporating these impurities decreases the overall fluid density in the pipeline and slows the pressure wave velocity. From an engineering perspective, introducing a moderate amount of gaseous impurities into a supercritical CO_2 pipeline can reduce the intensity of the pipeline water hammer.

4.2.3. Effect of Valve Closure Time and Mode on Pipeline Valve Water Strike. In addition to the medium's properties, the valve's operating behavior significantly influences the pipeline's water hammer phenomenon. To investigate the effects of different valve closure times and methods on water hammer fluctuations in CO_2 pipelines, we controlled the closure time by adjusting the valve opening as a function of time. We regulated the closure method by defining how the valve opening changes. Fox and Cheng argued that the closing effect of a valve cannot be reasonably discussed solely based on its opening and closing velocities without considering the pipeline cycle.[45] Consequently, based on the initial conditions, the range of pipeline cycles under the simulated conditions was between 44 and 57 s. Based on this result, several time-varying groups were chosen for the study. Simultaneously, by examining typical CCS projects—such as the Sleipner CO_2 storage project in Norway, the Quest Carbon Capture and Storage Facility in Canada, and the Gorgon CO_2 injection project in Australia—it was found that there are two main types of valve closure methods: linear closure and staged closure. These methods, whose different flow rate change rates result in varying water strike effects, were identified in these projects. Therefore, three types of closure, linear, fast-opening, and parabolic, were chosen to simulate different rates of flow change. Specifically, the linear type indicates a uniform change in flow rate; the fast-open type has a faster change in the initial period and a slower change in the later period, while the parabolic type has a slower change in the early period and a quicker change in the later period.

Figure 10a demonstrates the pressure fluctuation at the pipeline valve under the valve closing times of 20, 40, 60, and 80 s. With the extension of the valve shutoff time, the amplitude of the water strike pressure decreases, but the fluctuation frequency is unaffected by the valve shutoff time. In the case of a valve

https://doi.org/10.1021/acs.energyfuels.4c06010
Energy Fuels 2025, 39, 5463−5478

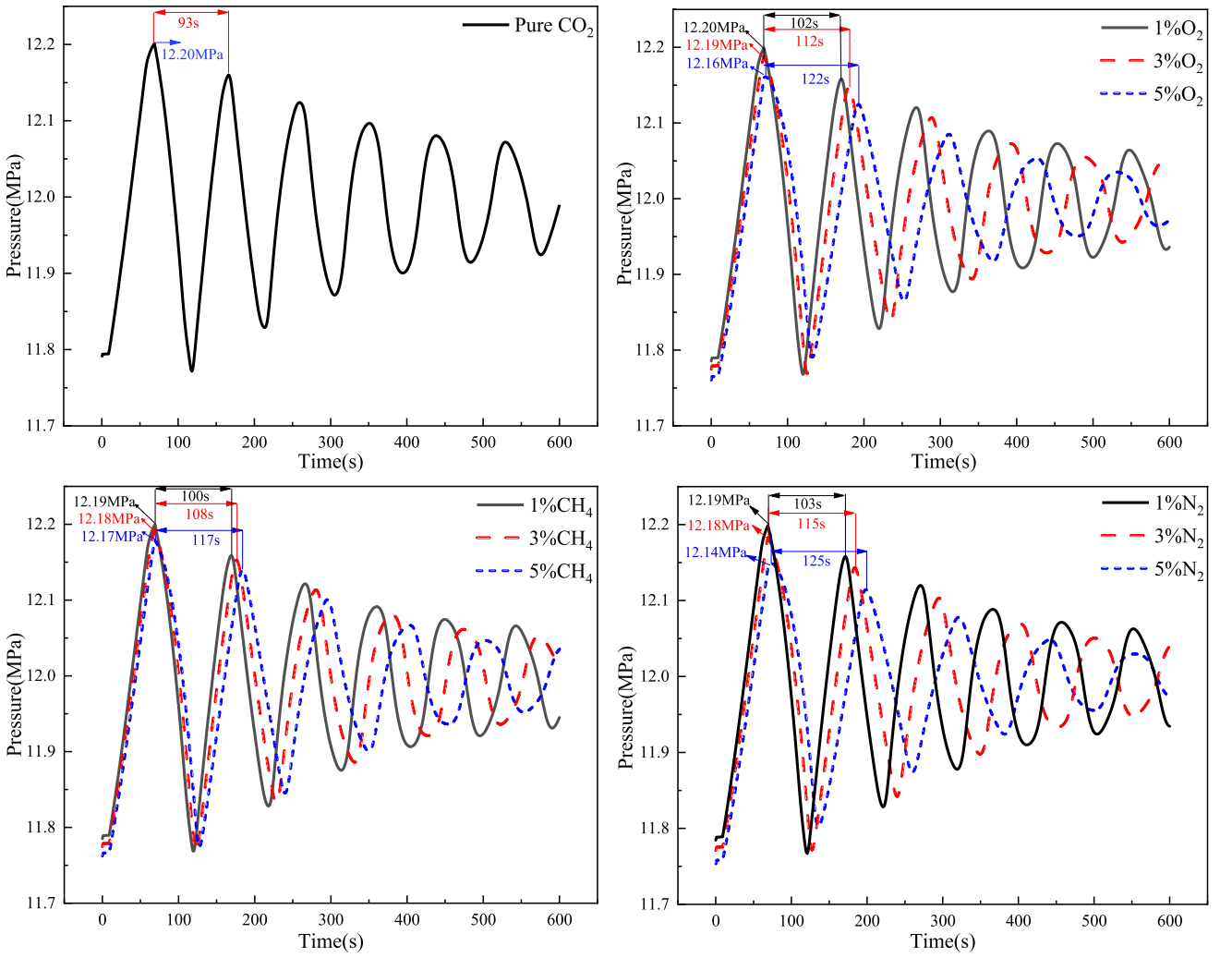

Figure 9. Effect of different impurities on the water strike of pipeline valves.

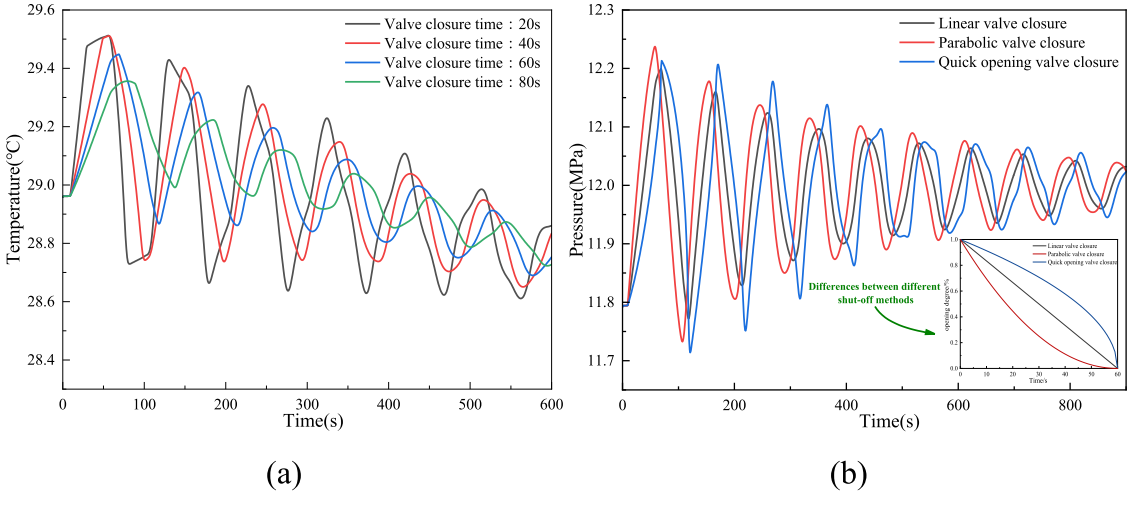

Figure 10. Effect of different valve operations on the water strike pressure in the pipeline: (a) valve closure time, (b) valve closure mode.

closing time of 80 s, the maximum water strike pressure was 0.33 MPa, which decreased by 28% compared to the case of a valve closing time of 20 s. This shows that extending the valve closing time significantly affects the pressure fluctuation at the pipeline valve. This indicates that the extended valve closing time effectively reduces the maximum water strike pressure.

From Figure 10b, it can be seen that there is a significant difference in the effect of different valve shutoff methods on water strikes in the pipeline. Regarding the time to reach the maximum water strike pressure, the parabolic shutoff valve has the fastest response, followed by the linear shutoff valve, while the fast-opening shutoff valve is the slowest. This is because the

https://doi.org/10.1021/acs.energyfuels.4c06010
Energy Fuels 2025, 39, 5463−5478

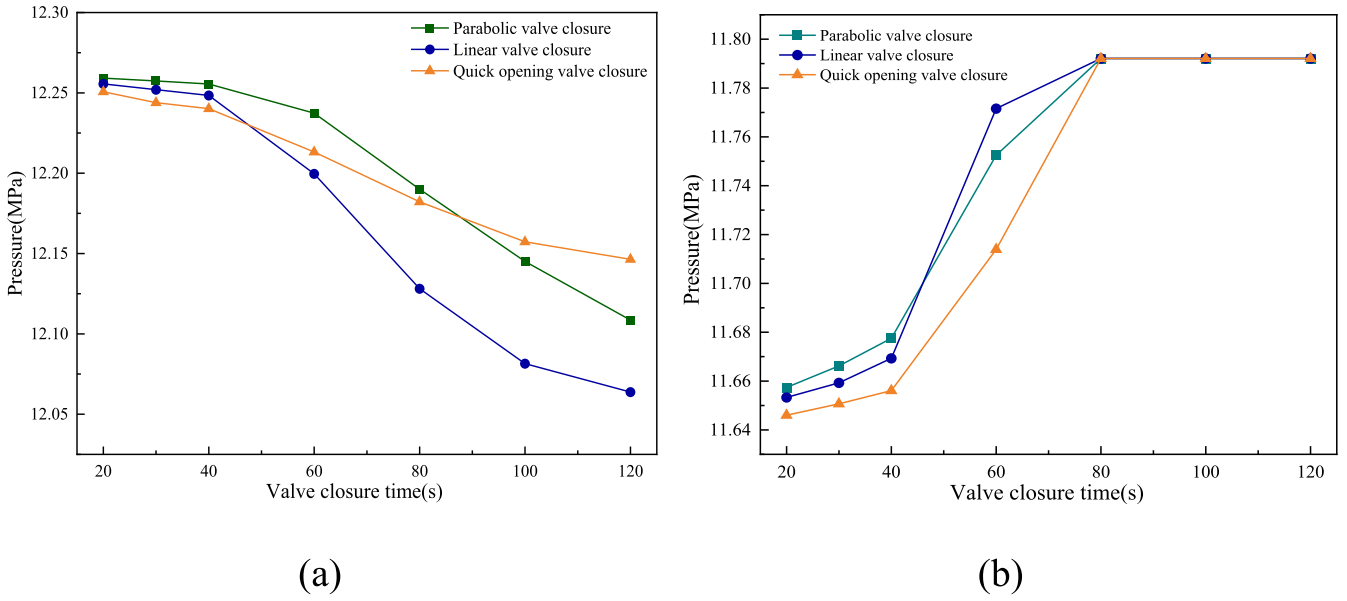

Figure 11. Maximum value of transient pressure at the valve at different closing times: (a) maximum value, (b) minimum value.

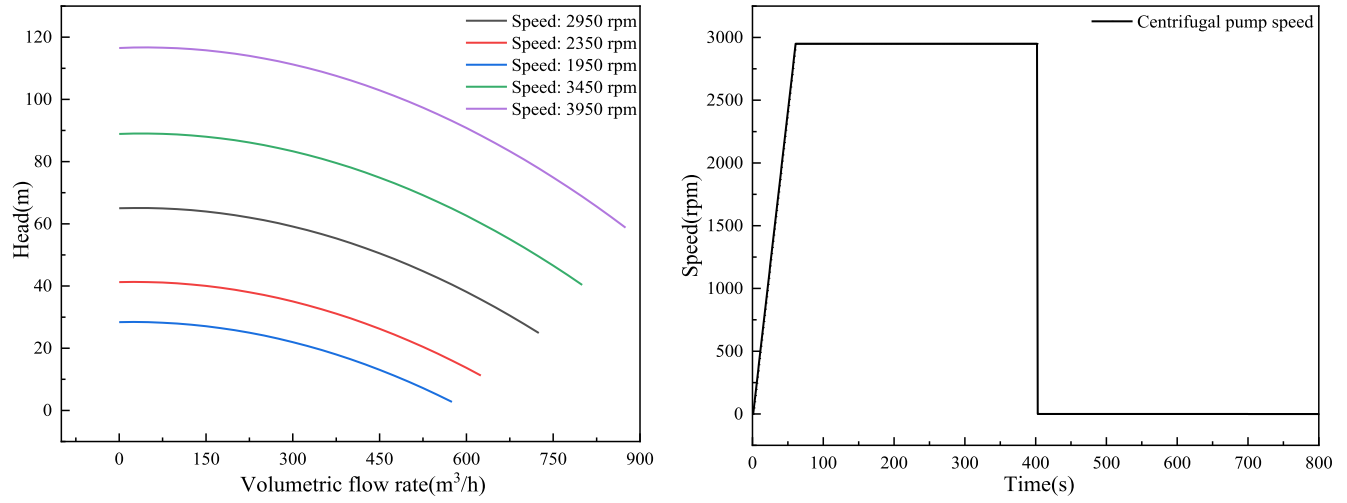

Figure 12. Schematic diagram of centrifugal pump parameters: (a) head-flow characteristic curve, (b) pump speed variation.

different shutoff methods cause the valve flow to drop to zero at different rates, with the illustrative shutoff valve being the fastest to close. Under the exact closing time conditions, the parabolic shutoff valve produces the highest maximum water strike pressure of 0.44 MPa, followed by the fast-open shutoff valve, and the linear shutoff valve is the lowest. This is due to the different flow rate changes caused by different valve shutoff methods, in which the rate of change of the linear valve is the most uniform and smooth, producing the lowest maximum water strike pressure. The other two types of closure result in a rapid change in the flow rate over a short period, resulting in a higher shock pressure.

To more clearly analyze the effect of the relationship between valve closing time and pipeline cycle on the water hammer and incorporate different valve closing methods, we simulated the maximum pressure under various operating conditions, as shown in Figure 11. The maximum water hammer pressure is higher when the valve closing time is shorter than the pipeline cycle, and extending the valve closing time does not significantly reduce the pressure. This is because, at this point, a direct water hammer occurs, and the reflected wave at the pipe inlet has not yet reached the valve, causing the valve action to end prematurely. In this case, the water hammer pressure is only affected by changes in flow rate, medium density, and pressure wave velocity and is not influenced by the valve closing time. In contrast, when the valve closing time exceeds the pipeline cycle, the maximum water hammer pressure is lower, and extending the valve closing time significantly reduces the pressure. At this point, the reflected water hammer wave has reached the valve, and the wave propagates upstream before the valve closes out the reflected wave, reducing the intensity of the water hammer. Prolonged valve closing time allows more reflected pressure waves to reach the valve, reducing the water hammer pressure. Indirect water hammer pressure is affected by changes in flow rate, medium density, and pressure wave velocity and is closely related to the valve closing time. The minimum water hammer pressure also follows the same trend with varying valve closing times. This principle applies to different valve closure modes, and a linear valve closure can effectively reduce the indirect water hammer pressure. Combined with the requirements of the

https://doi.org/10.1021/acs.energyfuels.4c06010
Energy Fuels 2025, 39, 5463−5478

DNV-RP-F104 (2021) standard, the pipeline cycle should first be calculated, and the maximum permissible closing time should be determined by considering the maximum time limit for valve closure. During this time, priority should be given to ensuring that the valve shutoff time exceeds the pipeline cycle, with an appropriate extension of the valve shutoff time. Simultaneously, to reduce the maximum water strike pressure in the CO_2 pipeline, priority should be given to selecting the linear valve closure method, which has a lower flow rate fluctuation. If necessary, then a phased valve shutdown can be implemented.

4.3. Slow Start and Sudden Stop of Centrifugal Pumps. This section investigates the hydraulic and thermal changes in the pipeline induced by the slow startup and sudden shutdown of the centrifugal pump at the pipeline inlet in the same scenario as in Section 3.1. The base conditions are an inlet temperature of 40 °C, an inlet pressure of 12 MPa, and an outlet flow rate of 70 kg/s. The gas source medium comprises pure CO_2 and the O_2, CH_4, and N_2 mixtures. The start and stop of the pump are controlled by adjusting the rotational speed of the centrifugal pump, rated at 2950 rpm, and the maximal head is 65 m. The head-flow characteristic curve of the centrifugal pump and the relationship of the pump's rotational speed with the change of time are shown in Figure 12. During the simulation, the speed of the centrifugal pump increases linearly from 0 rpm at startup to 2950 rpm in 60 s. After reaching this speed, the centrifugal pump will keep the speed of 2950 rpm unchanged until the moment of 400 s. At this point, the centrifugal pump will stop immediately. At this point, the centrifugal pump will immediately shut down, and the speed will rapidly decrease to 0 rpm until the end of the simulation. The gas source pressure and user flow rate remain constant throughout the simulation.

Figure 13 illustrates the trend of the pipeline pressure change during the slow startup of a centrifugal pump for pure CO_2 and a CO_2 mixture doped with 5% of the aqueous w/v O_2, CH_4, and N_2. The pressure change curves for each conveyed medium indicate similar pipeline pressure trends. As the centrifugal pump speed gradually increases, the pipeline outlet pressure first changes and steadily increases, forming a pressurized wave propagating along the pipeline. As a result, the pressure rise at 5 km and 10 km along the pipeline is significantly delayed. Although the centrifugal pump reaches its rated speed of 2950 rpm within 60 s, the pipeline pressure has not yet reached its maximum value and will continue to rise before eventually stabilizing. This is because, despite the centrifugal pump speed stabilizing, the pipeline inlet flow increased dramatically during startup, differing significantly from the outlet flow and thus requiring time to reach a new flow balance. During this process, the centrifugal pump outlet flow gradually decreases, resulting in a slow increase in pressure. A comparison of the data for pure CO_2 and mixtures containing impurity CO_2 revealed that doping with 5% O_2, CH_4, and N_2 reduced the pressure increase during centrifugal pump startup. Specifically, the pressure increase of the CO_2 mixture containing 5% O_2 was 0.36 MPa, which was 12.93% less than that of pure CO_2; the rise in the CO_2 mixture containing 5% CH_4 was 0.37 MPa, which was 10.52% less than that of pure CO_2; and the increase of the CO_2 mixture containing 5% N_2 was 0.34 MPa, which was 17.05% less than that of pure CO_2. Additionally, doping with O_2, CH_4, and N_2 also prolonged the boosting reaction time at 5 and 10 km, with the N_2 impurity having the most significant effect, followed by the augmentation of the effect by the addition of the nanoparticles to O_2 and CH_2 having the most miniature effect.

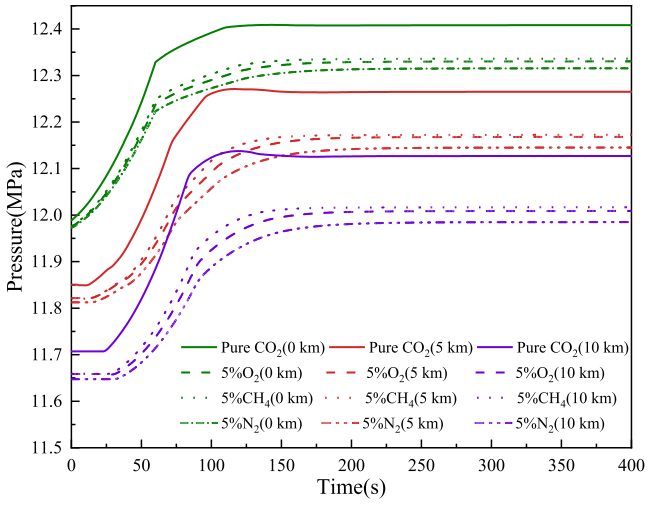

Figure 13. Trend of pipeline pressure under slow startup conditions for centrifugal pumps.

Figure 14 illustrates the distribution of pipeline parameters along the pipe for pure CO_2 and a CO_2 mixture doped with 5% O_2, CH_4, and N_2 at the 40th second, comparing it with the steady-state initial conditions. The calculations for different media show that the centrifugal pump startup increases the temperature, pressure, and mass flow rate parameters in the pipeline, with more minor changes in temperature and more significant changes in pressure and flow rate. Taking pure CO_2 as an example, the pressure along the pipeline generally increased by 0.05−0.17 MPa at the 40th second, demonstrating an apparent boosting effect. The change in flow rate along the pipeline is even more significant, with the centrifugal pump outlet flow rate increasing by 22.11 kg/s compared to that in the initial state, representing a boost of 31.58%. This indicates that the centrifugal pump startup causes a significant increase in the flow rate within the pipeline.

The effect of impurities on the centrifugal pump startup was derived by comparing the calculation results for pure CO_2 with those for mixtures doped with 5% of the compounds containing O_2, CH_4, and N_2. First, adding impurities led to a decrease in the temperature drop and an increase in the pressure drop at the initial moment. Specifically, 5% of the O_2 impurities decreased the temperature drop along the pipeline by 1.30 °C and increased the pressure drop by 0.04 MPa; 5% of the CH_4 impurities decreased the temperature drop by 1.03 °C and increased the pressure drop by 0.04 MPa; and 5% of the N_2 impurities decreased the temperature drop by 1.29 °C and increased the pressure drop by 0.05 MPa. Second, the parameter variations during centrifugal pump startup showed that the presence of impurities delayed the rise in temperature, pressure, and flow in the pipeline. This reduced the increase in these parameters, with the influence following this order: $N_2 > CH_4 > O_2$.

Figures 15 and 16 show the flow and pressure in the pipeline as a function of time after a sudden shutdown of the centrifugal pump under pure CO_2 conditions. The effect of impurities is similar to that of the centrifugal pump startup, resulting in a more extended period of fluctuation and a reduction in the oscillation amplitude, and it is therefore not repeated here. Observation reveals that when the centrifugal pump at the inlet of the pipeline is shut down, the pressure and flow rate at the beginning of the pipeline downstream drop rapidly. Specifically,

https://doi.org/10.1021/acs.energyfuels.4c06010
Energy Fuels 2025, 39, 5463−5478

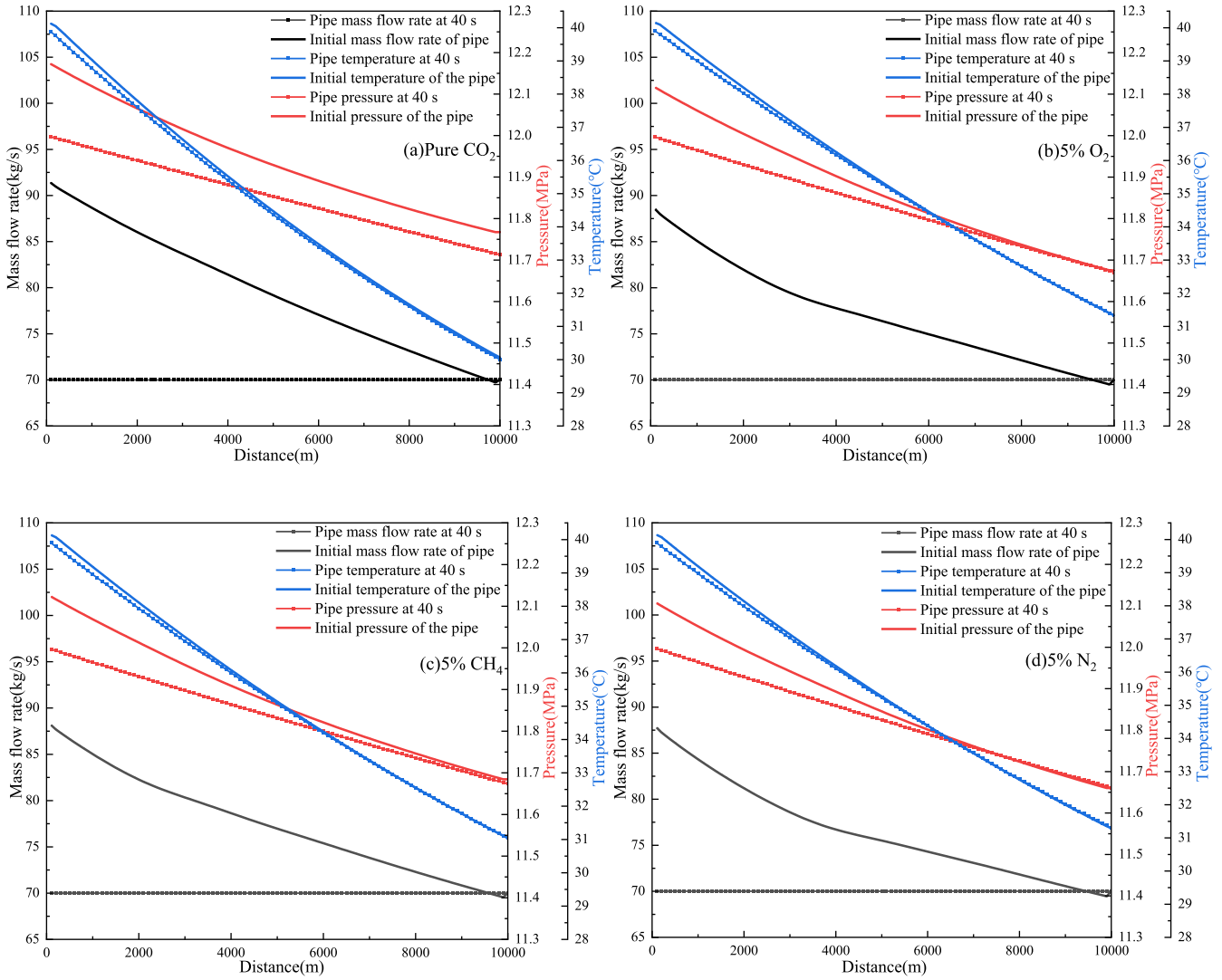

Figure 14. Schematic diagram of the pipeline's temperature, pressure, and flow rate distribution at the 40th s.

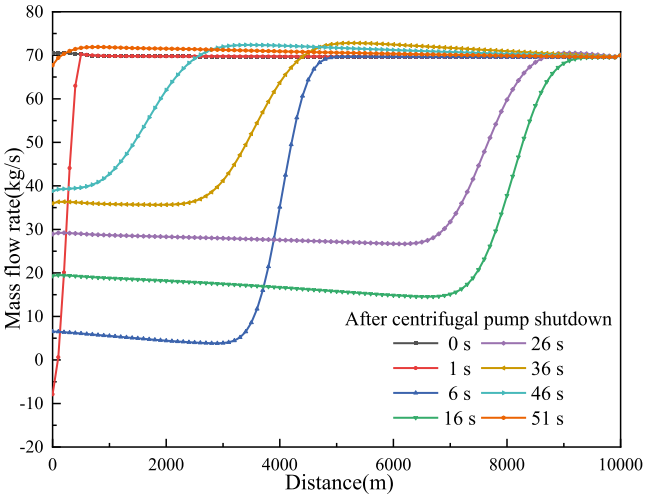

Figure 15. Mass flow rate changes at different moments after centrifugal pump shutdown.

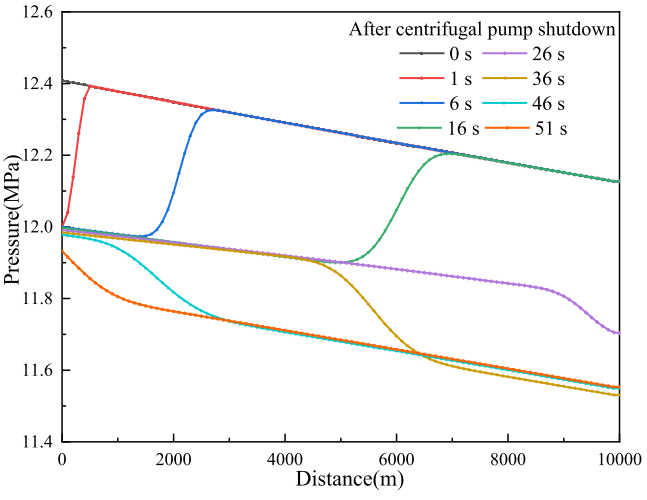

Figure 16. Pressure changes at different moments after centrifugal pump shutdown.

the pressure drops to 12 MPa, and the flow rate drops to almost zero. This trend of change propagated rapidly downstream into the pipeline. The effect reached the pipeline outlet at 16 s when the pressure and flow rate dropped significantly throughout the pipeline. Subsequently, as the flow in the pipeline is in a distribution imbalance and there is a flow differential, the flow

https://doi.org/10.1021/acs.energyfuels.4c06010
Energy Fuels 2025, 39, 5463−5478

begins to gradually flow back from the pipeline outlet toward the pipeline inlet. This process further caused the pressure along the pipeline to continue to drop. Eventually, at the 51st second, the piping system established a new equilibrium state after a dynamic evolution, and the flow rate and pressure were gradually restored to normal operating levels. The sudden stoppage of the centrifugal pump triggers a very rapid dynamic response in the piping system, resulting in significant flow and pressure changes, which may increase the risk of phase transitions and water strike phenomena and deserve attention.

5. CONCLUSIONS

In this study, we completed the transient modeling of the CO_2 pipeline using Visual Studio 2017 software and the C++ programming language and performed extensive numerical simulations and calculations. The study aims to describe the hydraulic and thermal response of a supercritical/dense-phase CO_2 pipeline under transient operating conditions, covering a variety of scenarios, such as valve closure, slow startup of centrifugal pumps, and sudden shutdown. The following conclusions were ultimately drawn:

(1) In this study, a one-dimensional nonisothermal transient flow model is developed for simulating the dynamic behavior of CO_2 pipelines. The GERG-2008 equation of state, which exhibits high accuracy in calculating CO_2 physical properties, was chosen by comparing it with the density experimental data in references. By comparing and analyzing the data with three sets of literature data from Liljemark S, Abbaspour M, and Adamkowski A, the results show that the computational results of the model developed in this paper are consistent with the literature data and show the same trend of change, and the error is within the acceptable range. This result verifies that the constructed transient model has high precision and accuracy and can meet the practical needs of engineering calculation.

(2) Under the same operating conditions, the maximum water strike pressure in a supercritical CO_2 pipeline is only one-third of that in a water pipeline but 12 times that in a methane pipeline. At the same time, the water strike fluctuation period in a supercritical CO_2 pipeline is 3 times that in a water pipeline and is close to that of a methane pipeline. Unlike standard gas pipelines, water strike in supercritical CO_2 pipelines requires special attention. The type and amount of impurities in CO_2 significantly affect the degree of water striking in the pipeline, with N_2 impurities having the most significant impact. When the N_2 content reaches 5%, the maximum water strike pressure decreases by 15.1%, while the fluctuation period of the water strike increases by 35.4%. In supercritical CO_2 pipelines, moderate doping of gas impurities can effectively reduce the intensity of water strikes.

(3) Different valve shutoff operations significantly impact water strikes in CO_2 pipelines. Regarding valve shutoff time, when the shutoff time is shorter than the pipeline cycle, the direct water strike pressure is more significant. It does not decrease with an increase in shutoff time. In contrast, when the shutoff time is longer than the pipeline cycle, the indirect water strike pressure is smaller and gradually decreases with increasing shutoff time. Regarding valve closing methods, linear valve closing can effectively reduce the intensity of valve water strikes. To ensure the safety of CO_2 pipelines, it is recommended that the valve shutoff time be greater than the pipeline cycle and appropriately extended, with preference given to linear shutoff valves.

(4) When the centrifugal pump at the pipeline inlet started slowly, the CO_2 pipeline inlet pressure and flow rate increased rapidly and propagated along the pipeline. In particular, the inlet flow rate changed significantly, increasing by 33.33% within 40 s of the centrifugal pump startup. In contrast, the sudden shutdown of the centrifugal pump caused a rapid and significant drop in flow and pressure in the pipeline system. At the moment of shutdown, the pipeline outlet pressure rapidly dropped to the gas source level, and the flow rate fell to nearly zero. This change propagated downstream and reached a new equilibrium state after 51 s. Impurities also significantly affect pressure changes in the tube, and doping reduces the magnitude and rate of pressure changes. To ensure the stability and efficiency of CO_2 fluid transfer, it is recommended that pipeline pressure and flow rate be monitored after centrifugal pump startup and shutdown to prevent phase change and water strike phenomena, thereby avoiding equipment damage.

AUTHOR INFORMATION

Corresponding Authors

Yuxing Li − *China University of Petroleum (East China), Qingdao, Shandong 266580, PR China*; Email: liyx@upc.edu.cn

Qihui Hu − *China University of Petroleum (East China), Qingdao, Shandong 266580, PR China*; orcid.org/0009-0004-2553-5308; Email: 2633151580@qq.com

Authors

Qiyun Jia − *China University of Petroleum (East China), Qingdao, Shandong 266580, PR China*

Xuefeng Zhao − *State Key Laboratory of Continental Shale Oil, PetroChina Daqing Oilfield Co, Daqing, Heilongjiang 163458, PR China*

Buze Yin − *China University of Petroleum (East China), Qingdao, Shandong 266580, PR China*

Lan Meng − *State Key Laboratory of Continental Shale Oil, PetroChina Daqing Oilfield Co, Daqing, Heilongjiang 163458, PR China*

Jianlu Zhu − *China University of Petroleum (East China), Qingdao, Shandong 266580, PR China*

Jianxin Lu − *Technische Universiteit Delft, Delft 2628, The Netherlands*

Complete contact information is available at: https://pubs.acs.org/10.1021/acs.energyfuels.4c06010

Notes

The authors declare no competing financial interest.

ACKNOWLEDGMENTS

This work was supported by the Heilongjiang Provincial Nature Fund (no. ZD2024E010).

NOMENCLATURE

Alphabetical nomenclature

A area [m^2]

https://doi.org/10.1021/acs.energyfuels.4c06010
Energy Fuels 2025, 39, 5463−5478

A_f valve overflow area [m^2]
a pressure wave velocity [m/s]
a_s sound speed [m/s]
C_d valve flow coefficient
C_p specific heat capacity [J/kg·K]
D diameter [m]
D_{in} valve inlet Joule−Thomson coefficient [K/MPa]
D_{out} valve outlet Joule−Thomson coefficient [K/MPa]
E modulus of elasticity of pipes [pa]
e thickness [m]
g gravity constant = 9.81 [m/s^2]
h enthalpy [J/kg]
K total heat transfer coefficient [$W/(m^2 \cdot K$]
L pipe length [m]
R partial derivative of a differential equation
m mass flow rate [kg/s]
N actual pump speed [rpm]
N_{rate} rated pump speed [rpm]
p gas pressure [pa]
q heat exchange rate [J]
Q valve volume flow rate [m^3/h]
Q_v volume displacement of the pump [m^3/h]
s pipe elevation [m]
T gas temperature [K]
u internal energy [J/kg]
υ specific volume [m^3/kg]
x pipe axial length [m]
y bed layer height [m]

Greek letter nomenclature

ρ density [kg/m^3]
τ time-variant [s]
λ coefficient of friction
v flow rate [m/s]
β_p coefficient of thermal expansion [1/K]

Subscripts

amb pipes buried deep
i upper layer
in inlet
j down layer
k pacemaker
out outlet

REFERENCES

(1) Bose, D.; Bhattacharya, R.; Kaur, T.; et al. Innovative Carbon Capture and Storage Approaches Are Crucial Measures for Emission Reduction within Industrial Sectors. *Carbon Capture Sci. Technol.* **2024**, *12*, 100238.
(2) Miao, L.; Feng, L.; Ma, Y. Comprehensive Evaluation of CCUS Technology: A Case Study of China's First Million-Tonne CCUS-EOR Project. *Environ. Impact Assess. Rev.* **2025**, *110*, 107684.
(3) Mim, R. T.; Negash, B. M.; Jufar, S. R.; et al. Minireview on CO_2 Storage in Deep Saline Aquifers: Methods, Opportunities, Challenges, and Perspectives. *Energy Fuels* **2023**, *37* (23), 18467−18484.
(4) Li, X. Z.; Yuan, L.; Zhang, C. Research Progress and Direction on Transient Transportation Process of Supercritical CO_2 Pipeline. *Petrol. Geol. Oilfield Dev. Daqing* **2024**, *43* (1), 22−32.
(5) Huang, W. H.; Li, Y. X.; Cheng, P. C. China's CO_2 Pipeline Development Strategy under the Strategy of Carbon Neutrality. *Nat. Gas Ind. B* **2023**, *43* (7), 1−9.
(6) Zhang, Z. X.; Wang, G. X.; Massarotto, P.; et al. Optimisation of Pipeline Transport for CO_2 Sequestration. *Energy Convers. Manage.* **2006**, *47* (6), 702−715.
(7) Du, Y.; Liu, L.; Liao, G.; et al. Density Fluctuations and Transport Properties of Supercritical Carbon Dioxide Calculated by Molecular Dynamics Simulation near the Widom Line. *J. Supercrit. Fluids* **2023**, *200*, 106003.
(8) Munkejord, S. T.; Hammer, M.; Løvseth, S. W. CO2 Transport: Data and Models-A Review. *Appl. Energy* **2016**, *169*, 499−523.
(9) Lu, J. X.; Hu, Q. H.; Zhang, D. H.; et al. Numerical Simulation of Impurity-Containing Supercritical CO_2 Pipeline Transport in CCUS. *Int. J. Greenhouse Gas Control* **2024**, *138*, 104236.
(10) McCoy, S. T.; Rubin, E. S. An Engineering-Economic Model of Pipeline Transport of CO_2 with Application to Carbon Capture and Storage. *Int. J. Greenhouse Gas Control* **2008**, *2* (2), 219−229.
(11) Nimtz, M.; Klatt, M.; Wiese, B.; et al. Modelling of the CO_2 Process-and Transport Chain in CCS Systems—Examination of Transport and Storage Processes. *Geochem.* **2010**, *70*, 185−192.
(12) Liu, X. *Thermodynamic and Hydraulic Numerical Calculation and Applications of Two Phases Flow in Horizontal Gathering Line under Carbon Dioxide*; Northeast Petroleum University, 2013.
(13) Liu, M.; Teng, L.; Li, Y. X.; et al. Study on Hydraulic Model and Characteristics for Supercritical CO_2 Pipelines. *Oil-Gas Field Surf. Eng.* **2016**, *35* (6), 14−17.
(14) Lu, J. X.; Hou, L.; Wang, Y. J. Characteristics and Economics of Supercritical CO_2 Pipeline Transportation in Undulating Terrain. *Nat. Gas Chem. Ind.* **2021**, *46* (01), 121−127.
(15) Mahgerefteh, H.; Oke, A. O.; Rykov, Y. Efficient Numerical Solution for Highly Transient Flows. *Chem. Eng. Sci.* **2006**, *61* (15), 5049−5056.
(16) Munkejord, S. T.; Jakobsen, J. P.; Austegard, A.; et al. Thermo- and Fluid-Dynamical Modelling of Two-Phase Multi-Component Carbon Dioxide Mixtures. *Int. J. Greenhouse Gas Control* **2010**, *4* (4), 589−596.
(17) Brown, S.; Martynov, S.; Mahgerefteh, H.; et al. Modelling the Non-Equilibrium Two-Phase Flow during Depressurisation of CO2 Pipelines. *Int. J. Greenhouse Gas Control* **2014**, *30*, 9−18.
(18) Quinn, D.; Stannard, D.; Edwards, J.; et al. Experimental Visualisation and Characteristics of Bubble Nucleation during Rapid Decompression of Supercritical and Subcooled Carbon Dioxide. *Int. J. Pressure Vessels Pip.* **2022**, *195*, 104569.
(19) Clausen, S.; Oosterkamp, A.; Strøm, K. L. Depressurization of a 50 km Long 24 Inches CO_2 Pipeline. *Energy Procedia* **2012**, *23*, 256−265.
(20) Shang, Y.; Chen, X.; Yang, M.; et al. Comprehensive Review on Leakage Characteristics and Diffusion Laws of Carbon Dioxide Pipelines. *Energy Fuels* **2024**, *38* (12), 10456−10493.
(21) Chen, L.; Hu, Y.; Liu, Z.; et al. Experimental Research on the Fracture and Arrest Process of Supercritical CO_2 Pipelines. *Int. J. Pressure Vessels Pip.* **2024**, *212*, 105314.
(22) Chaczykowski, M.; Osiadacz, A. J. Dynamic Simulation of Pipelines Containing Dense Phase/Supercritical CO_2-Rich Mixtures for Carbon Capture and Storage. *Int. J. Greenhouse Gas Control* **2012**, *9*, 446−456.
(23) Li, J. F.; Xu, K. T.; Xiao, H. Numerical Simulation of CO_2 Pipeline Based on Span-Wagner EOS. *Bull. Sci. Technol.* **2017**, *33* (5), 10−15.
(24) Arai, Y.; Kaminishi, G. I.; Saito, S. The Experimental Determination of the PVTX Relations for the Carbon Dioxide-Nitrogen and the Carbon Dioxide-Methane Systems. *J. Chem. Eng. Jpn.* **1971**, *4* (2), 113−122.
(25) Magee, J. W.; Ely, J. F. Isochoric, (p v T) Measurements on CO2 and (0.98 CO2 + 0.02 CH4) from 225 to 400 K and Pressures to 35 MPa. *Int. J. Thermophys.* **1988**, *9*, 547−557.
(26) Brugge, H. B.; Holste, J. C.; Hall, K. R.; et al. Densities of Carbon Dioxide + nitrogen from 225 to 450 K at Pressures up to 70 MPa. *J. Chem. Eng. Data* **1997**, *42* (5), 903−907.
(27) Klimeck, J.; Kleinrahm, R.; Wagner, W. Measurements of the (p, ρ, T) Relation of Methane and Carbon Dioxide in the Temperature Range 240 to 520 K at Pressures up to 30 MPa Using a New Accurate Single-Sinker Densimeter. *J. Chem. Thermodyn.* **2001**, *33* (3), 251−267.
(28) Saleh, B.; Wendland, M. Measurement of Vapor Pressures and Saturated Liquid Densities of Pure Fluids with a New Apparatus. *J. Chem. Eng. Data* **2005**, *50* (2), 429−437.

https://doi.org/10.1021/acs.energyfuels.4c06010
Energy Fuels 2025, 39, 5463−5478

(29) Mazzoccoli, M.; Bosio, B.; Arato, E. Analysis and Comparison of Equations-of-State with p-ρ-T Experimental Data for CO_2 and CO_2-Mixture Pipeline Transport. *Energy Procedia* **2012**, *23*, 274−283.
(30) Mondéjar, M. E.; Villamañán, R. M.; Span, R.; et al. Accurate (p, ρ, T) data for two new (carbon dioxide+ nitrogen) mixtures from (250 to 400) K at pressures up to 20 MPa. *J. Chem. Thermodyn.* **2012**, *48*, 254−259.
(31) Kunz, O.; Wagner, W. The GERG-2008 Wide-Range Equation of State for Natural Gases and Other Mixtures: An Expansion of GERG-2004. *J. Chem. Eng. Data* **2012**, *57* (11), 3032−3091.
(32) Gernert, J.; Span, R. E. O. S. −C. G. EOS−CG: A Helmholtz energy mixture model for humid gases and CCS mixtures. *J. Chem. Thermodyn.* **2016**, *93*, 274−293.
(33) Fenghour, A.; Wakeham, W. A.; Vesovic, V. The Viscosity of Carbon Dioxide. *J. Phys. Chem. Ref. Data* **1998**, *27* (1), 31−44.
(34) Vesovic, V.; Wakeham, W. A.; Olchowy, G. A.; et al. The Transport Properties of Carbon Dioxide. *J. Phys. Chem. Ref. Data* **1990**, *19* (3), 763−808.
(35) Mahgerefteh, H.; Oke, A.; Atti, O. Modelling Outflow Following Rupture in Pipeline Networks. *Chem. Eng. Sci.* **2006**, *61* (6), 1811−1818.
(36) Chen, J. T.; Chang, M. H.; Chen, K. H.; et al. The Boundary Collocation Method with Meshless Concept for Acoustic Eigenanalysis of Two-Dimensional Cavities Using Radial Basis Function. *J. Sound Vib.* **2002**, *257* (4), 667−711.
(37) Liljemark, S.; Arvidsson, K.; McCann, M. T. P.; et al. Dynamic Simulation of a Carbon Dioxide Transfer Pipeline for Analysis of Normal Operation and Failure Modes. *Energy Procedia* **2011**, *4*, 3040−3047.
(38) Abbaspour, M.; Chapman, K. S. Non-isothermal Transient Flow in Natural Gas Pipeline. *J. Appl. Mech.* **2008**, *75* (3), 519−525.
(39) Adamkowski, A.; Lewandowski, M. Experimental Examination of Unsteady Friction Models for Transient Pipe Flow Simulation. *J. Fluids Eng.* **2006**, *128* (6), 1351−1363.
(40) Bai, F.; Lu, Y. Effects of Impurities on Anthropogenic CO_2 Pipeline Transport. *Energy Fuels* **2024**, *38* (11), 9958−9966.
(41) De Visser, E.; Hendriks, C.; Barrio, M.; et al. Dynamis CO_2 Quality Recommendations. *Int. J. Greenhouse Gas Control* **2008**, *2* (4), 478−484.
(42) Porthos CO2 Transport and Storage. *Standard CO2 Transport and Storage Conditions*, 2021.
(43) Shirley, P.; Myles, P. *Quality Guidelines for Energy System Studies: CO_2 Impurity Design Parameters*; National Energy Technology Laboratory (NETL): Pittsburgh, PA, Morgantown, WV, and Albany, OR (United States), 2019.
(44) ISO N. *Carbon Dioxide Capture, Transportation and Geological Storage−Pipeline Transportation Systems*, 2016.
(45) Fox, J. A.; Cheng, Z. Z. *Hydraulic Analysis of Unsteady Flow in Pipe Networks*; Petroleum Industry Press, 1983.

https://doi.org/10.1021/acs.energyfuels.4c06010
Energy Fuels 2025, 39, 5463−5478